TELKOMNIKA, Vol. 11, No. 10, October 2013, pp. 6017 ~ 6024
ISSN: 2302-4046

Optimization and Construction of Single-side Nuclear Magnetic Resonance Magnet

Ji Yongliang*, He Wei, He Xiaolong
State Key Laboratory of Power Transmission Equipment & System Security and New Technology, Chongqing University, Chongqing 400030, China,
*Corresponding author, e-mail: jiyongliang@gmail.com

Abstract

Single-sided NMR devices can operate under conditions inaccessible to conventional NMR while featuring portability and the ability to analyze arbitrary-sized objects. In this paper, a semi-elliptic Halbach magnet array was designed and built for single-side Nuclear Magnetic Resonance (NMR). We present an easy-to-implement target field algorithm for single-side NMR magnet design based on Gram-Schmidt Orthogonal method. The creating magnetic field of designed magnet structure could achieve best flatness in the region of interesting for NMR applications. The optimizing result shows that the best magnet structure can generate magnetic fields which flatly distributed in the horizontal direction and the gradient was distributed in the vertical direction with gradient of 2mT/mm. The field strength and gradient were measured by a three dimensions Hall probe and agreed well with the simulations.

Keywords*: single-side magnet, Nuclear Magnetic Resonance, curve fitting, optimization design*

1. Introduction

Compared with the traditional enclosed nuclear magnetic resonance (NMR) equipment, unilateral nuclear magnetic resonance equipment scan objects from the surface without encompassing them [1, 2]. At the same time, its volume is small and portable, so it has been widely used in food analysis and quality control, material science, physical geography, etc.[3-9]. In unilateral nuclear magnetic resonance equipment, the generation of its main magnetic field depends on the permanent magnet. The typical magnet structures include U shape magnet [10], Halbach array [11, 12], and barrel-shape magnet etc. At the same time, permanent magnets also have been used to generate gradient magnetic field. In the literature [10], it is pointed out that single strip magnet has good gradient magnetic field characteristics in a distance along the magnetization direction of the upper and lower surface centers. On the basis of supposing high-permeability material surface as an equal scalar magnetic potential face, a type of magnet structure with horizontally uniform magnetic field while vertically gradient magnetic field was constructed by means of separation of variables [13].

The currently design of unilateral nuclear magnetic resonance magnet needs extra gradient coils due to lack of gradient magnetic field. However, the design theory of gradient coils for unilateral nuclear magnetic resonance is still not mature. The magnet designed through method of separation of variables can generate gradient magnetic field but its enclosed structure makes it hard to apply in unilateral nuclear magnetic resonance.

In the paper, we proposed improvement and optimization on the traditional Halbach magnet structure through the curve fitting method and obtained a new unilateral magnet structure. The designed magnet array can generate magnetic field with sound flatness in horizontal direction and gradient in vertical direction in a specific area. So the designed magnet structure does not need extra gradient coils [14], which simplified the gradient coding system design.

2. Calculation of the Magnetic Field

The calculation of the magnetic field of permanent magnet adopts scalar magnetic potential method on the basis of magnetic charge theory. In order to improve the calculation

Received April 18, 2013; Revised July 11, 2013; Accepted July 21, 2013

accuracy, this paper made use of second order finite element algorithm [15] and obtained the following finite element equation,

$$K\varphi = R \tag{1}$$

$$K_{ij} = \int_{V_e} \mu \nabla N_i \cdot \nabla N_j dV, i, j \in 1,2...10 \tag{2}$$

$$R_i = \int_{S_e} \vec{n} \cdot \vec{B}_r N_i ds \qquad i \in 1,2...6 \tag{3}$$

where *n* represents the outward unit normal vector on the surface of the magnet, ***B****r* is the residual magnetism of the magnet, *Ni* is the shape function of second order tetrahedron element. After solving the scalar magnetic potential *φ,* the magnetic field distribution around the space of permanent magnet can be got.

3. Design of Unilateral Magnet Structure

Due to the generation of uniform magnetic field in its cylindrical cavity, Halbach magnet is has been paid great attention to. Figure 1(a) shows Halbach magnet constructed by 16 magnetic bars with the same shape and residual magnetism [11]. However, its structure is enclosed, which makes it difficult to be applied in unilateral nuclear magnetic resonance. For this reason, the below 9 magnetic bars is remained (Figure 1(b)).

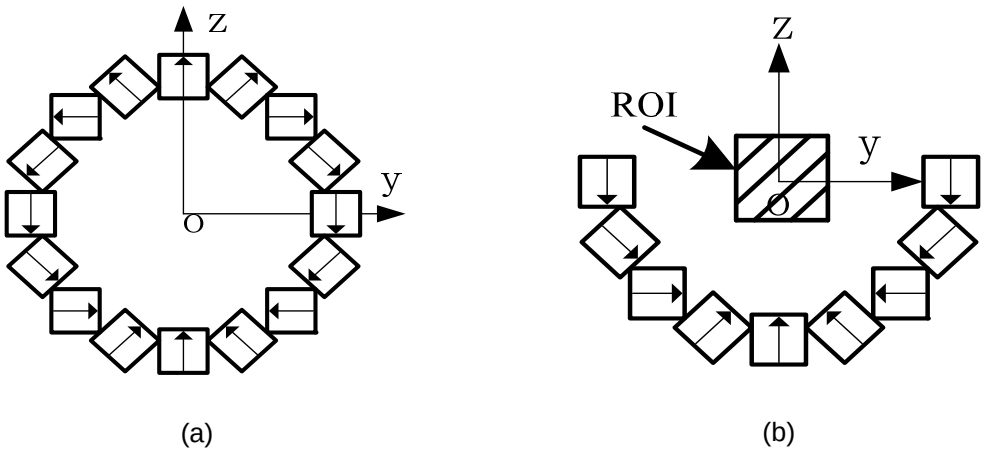

(a) (b)

Figure 1. (a)Halbach magnet array. (b) Single-side magnet array.

The magnet size is 3 cm × 3 cm × 10 cm, *Br* is 1.28T. The arrow is the direction of bar magnet magnetization. In YOZ plane, Figure 3 shows the Z-component of magnetic flux density in region of interesting (ROI) in a square area of 5cm length (Figure 2).

From Figure 2, it can be seen that the magnetic field presents gradient approximation changes along Z axis and equipotential line sags to the negative direction of Z axis. The reason for this is due to the closer distance from point 1 and point 3 to the magnet, where the magnetic field is strong while the further distance from point 2 to the magnet, where the magnetic field is weak. Therefore, we can deduce that if move the magnets in Figure 1(b) on the both sides to the center of Y and move down the magnet, the magnet equipotential line in ROI area will sag more sharply, shown as Figure 4. For this specific move, please refer to Figure 3. If performing the reverse operation on the magnet in Figure 1(b), the magnet equipotential line in ROI area will sag towards the upper side of Z axis (see in Figure 5).

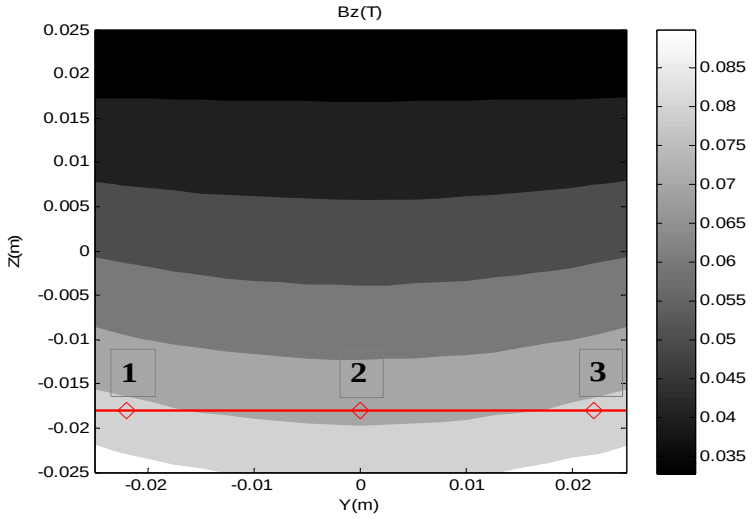

Figure 2. The Z-component of magnetic flux density in ROI.

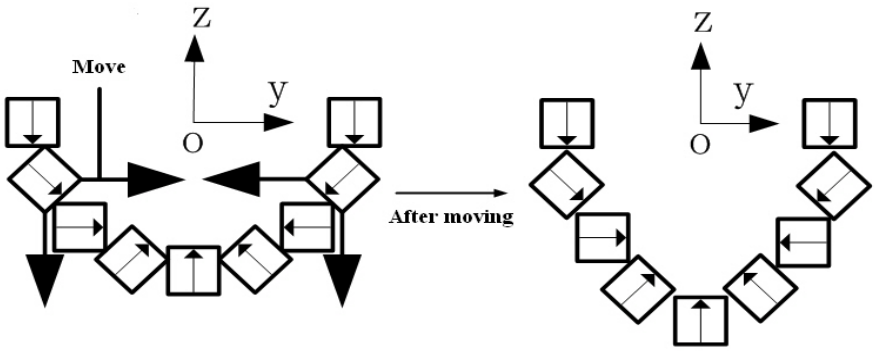

Figure 3. Moving operation of magnet array.

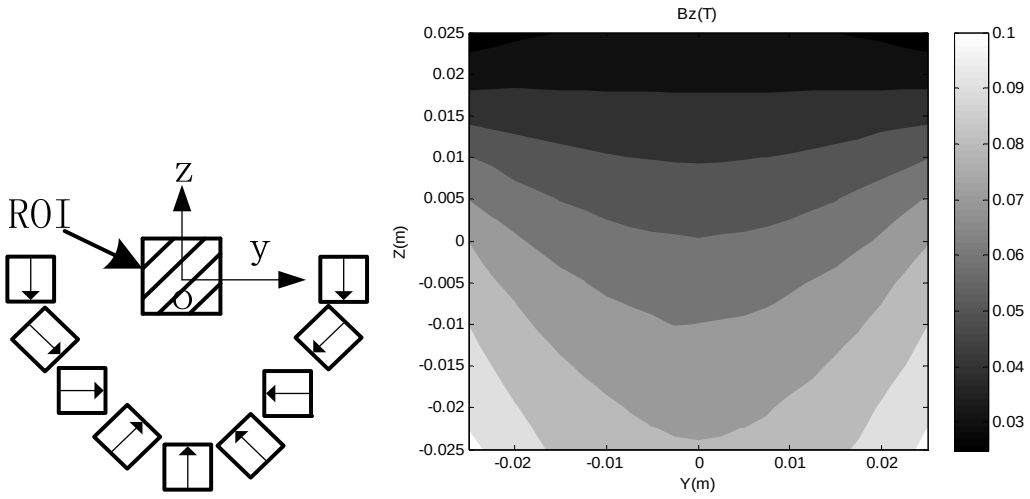

Figure 4. The moved magnet array and its magnetic field in ROI.

Therefore, inevitably there is a condition under which the magnetic equipotential line in ROI has best flatness and gradient approximation distribution characteristics. This kind of magnet structure and magnetic field is what the unilateral nuclear magnetic resonance needs.

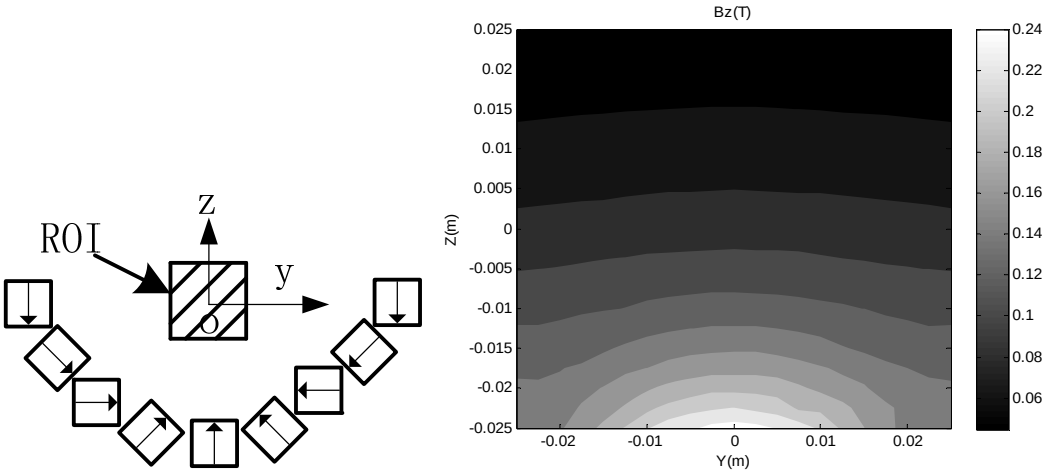

Figure 5. The reverse operated magnet array and its magnetic field in ROI.

4. Optimization of Magnet Structure

In terms of different magnet structures, the elliptic curve can be used to simulate. Put the magnet equal arc length on the elliptic curve and change the magnet structure by adjusting the length of elliptic semi-major axis.

The elliptic equation in YOZ plane is shown as

$$\frac{y^2}{a^2}+\frac{z^2}{b^2}=1 \tag{4}$$

where *a, b* represent the lengths of elliptic semi-major axis and semi-minor axis, respectively. To facilitate the optimization of magnet structure, the following constraint condition is added.

$$a \cdot b = r \cdot \ r = r^2 \tag{5}$$

r represents the radius of the circle where the center of Halbach magnet is located, thus the magnet structure is determined by *a*. When $a < b$, $a = b = r$ and $a > b$, three magnet structures in above section can be realized respectively.

In order to describe the flatness of equipotential line, choose 21 equal-interval segments in the ROI along Z axis. In each segment, select 21 equal-interval points. In this way, 441 grid points are formed. Then we calculated the magnetic field of Z-component of each point in each segment respectively. The flatness of the equipotential diagram in this area can be approximately represented by the following formula.

$$Std = \frac{1}{n}\sum_{i=1}^{n} std_i \tag{6}$$

$$std_i = \frac{1}{m}\sqrt{\sum_{j=1}^{m}(B_{zij}-\bar{B}_{iz})^2} \tag{7}$$

where B_{zij} is the magnetic field of Z-component of point *j* on segments *i*, B_{iz} is the mean magnetic field of Z-component of all field points on segment *i,* std_i is the standard variance of

magnetic field of Z-component of all field points on segment *i*, *Std* is the mean standard variance of all segments. So mean standard variance *Std* approximately represents the flatness of the equipotential line. The smaller the value is, the closer the value of the magnetic field Z axis component on all segments and the flatter the equipotential line is.

The semi-major axis was changed from 0.7*r* to 2*r* with step of 0.05*r.* Calculate mean standard variance *Std* of magnetic field of Z-component in ROI in each magnet structure, respectively. The drawn scatter diagram is as follows.

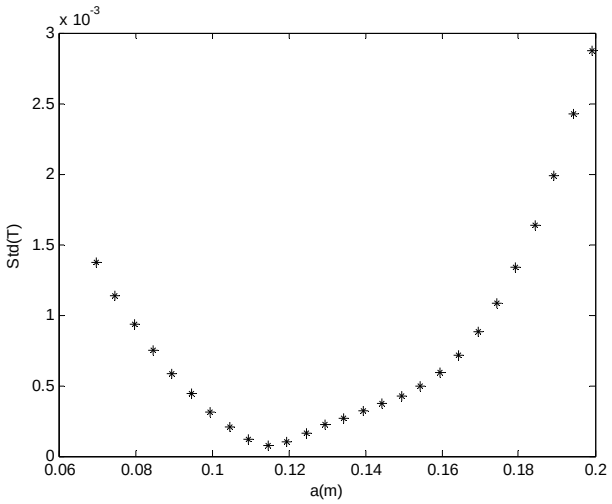

Figure 6. The scatter diagram of *Std* about *a*

It can be found that there exists the lowest point about mean standard variance *Std* in scatter diagram Figure 6. In order to find out the location of the lowest, this paper carried out fitting on the data points. The general polynomial for fitting will result in the fitting equation to present pathological characteristics, which will obtain large calculation error [16]. So this paper made use of Gram-Schmidt orthogonalization method to make curve fitting through.

Orthogonal polynomial can be obtained by following equation.

$$P_k = x^k - \sum_{j=0}^{k-1} \alpha_{jk} P_j(x), k = 0,1...m \tag{8}$$

$$\alpha_{jk} = \frac{\sum_{i=0}^{n} x^k P_j(x_i)}{\sum_{i=0}^{n} P_j^{\,2}(x_i)}, \begin{matrix} j = 0,1...k-1 \\ k = 0,1...m \end{matrix} \tag{9}$$

Fitting coefficient is

$$\alpha_j = \frac{\sum_{i=0}^{n} f_i P_j(x_i)}{\sum_{i=0}^{n} P_j^{\,2}(x_i)}, j = 0,1...m \tag{10}$$

Fitting equation is

$$y = \sum_{j=0}^{m} \alpha_j P_j(x) \tag{11}$$

5. Results and Discussions

Gradually improve the degree of fitting polynomial, we can find out the fitting equation satisfying the requirements of square error. In this paper, the requirement of fitting square error is less than 10-8. Then obtained fitting equation and the fitting curve are shown as below (Figure 7)

$$\begin{aligned} Std = & -242676.4a^7 + 213909a^6 \\ & -78124.2a^5 + 15294.2a^4 - 1730.7a^3 \\ & +113.55a^2 - 4.06a + 0.0838 \end{aligned} \tag{12}$$

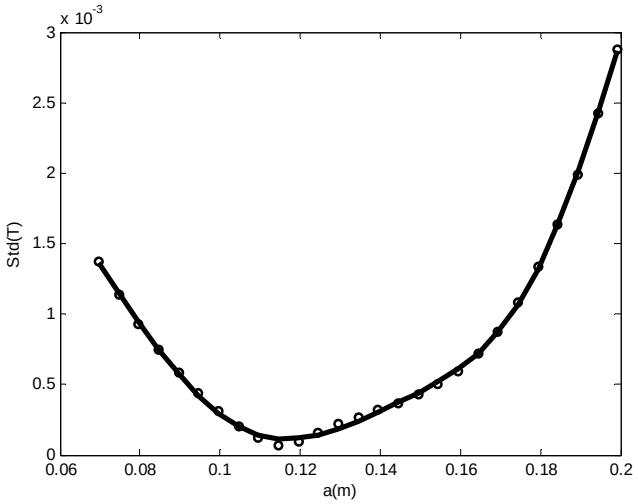

Figure 7. The fitting curve of *Std* about *a*

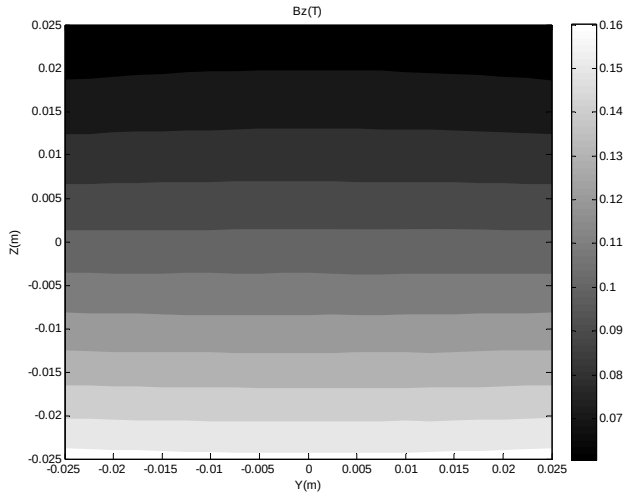

Figure 8. The simulated magnetic field distribution of optimized magnet array.

Taken the derivative of fitting Equation (12) with respect to variable ***a***, the value of variable ***a*** can be obtained corresponding to the lowest position in fitting curving. The equipotential of the corresponding magnetic field Z-component B_z is shown as below (Figure 8).

According to the above designed magnet parameter, the experimental magnet array was constructed (see Figure 9(a)). A motor-driven three-dimensional magnetic field measuring platform (see Figure 9(b)) was used to measure the magnetic field in ROI area generated by magnet array. The measured results were shown as Figure 10(a) and Figure 10(b).

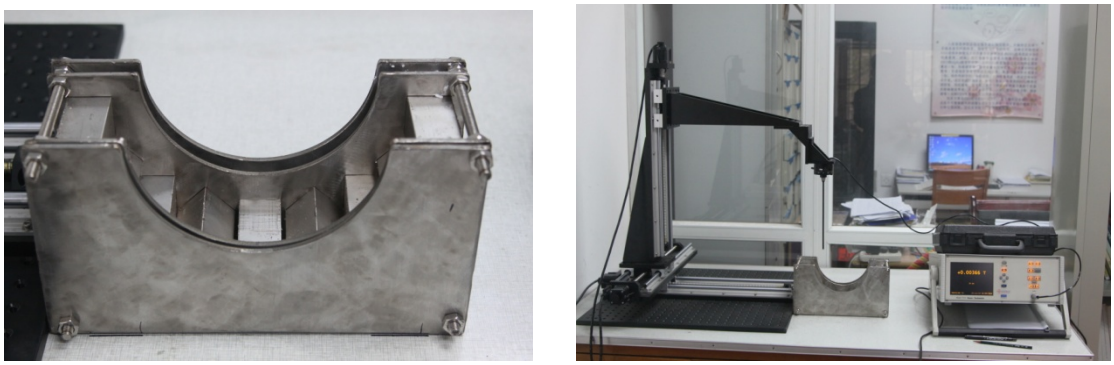

Figure 9. (a)The prototype of optimized magnet array. (b)The motor-driven three-dimensional magnetic field measuring platform

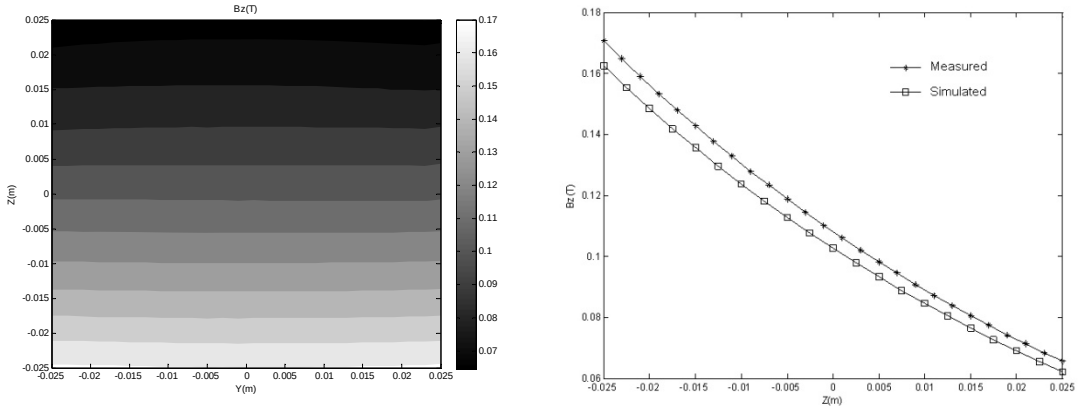

Figure 10. (a) The measured magnetic field distribution of optimized magnet array. (b) The value of simulated and measured magnetic flux ***Bz***

According to the simulation and measurement results, it can be seen that both simulation calculation value and measured value of magnetic field Z axis component have good flatness and magnet gradient along Z axis (2mT/mm), simultaneously.

At the same time, carry out simulation calculation on Z plane magnet field at different height. We found that at the height of Z = 17 mm, within the box of (-2mm, 2mm)×(-2mm, 2mm), the magnetic field is relatively uniform and uniformity is 1300 ppm and field strength is 0.0739T.

6. Conclusion

On the basis of the improvement and optimization of single-side (unilateral) Halbach magnet structure, this paper obtained and constructed a new unilateral Halbach structure array according to the optimization results. The results of the simulation calculation and actual measurement of the magnetic field both indicated that the magnet has better flatness and

gradient (2mT/mm) in area of 50 mm × 50 mm. The uniformity in ROI area of 4 mm × 4 mm is 1300 ppm and its field strength is 0.0739T.

References

[1] Wei-Hao Chang, Jyh-Horng Che. Single-side mobile NMR apparatus using the transverse flux of a single permanent magnet. *Magnetic Resonance Imaging.* 2009; 24:123-133.
[2] VA Demas, PJ Prado. Compact Magnets for Magnetic Resonance. *Concepts in Magnetic Resonance PartA*. 2009; 32A: 48-59.
[3] Elena Badea, L Miu. Study deterioration of historical parchments by various thermal analysis techniques complemented by fire, UV–VIS–NIR and unilateral NMR investigations. *Journal of Thermal Analysis and Calorimetry*. 2009; 91:17-27.
[4] D Capitani, N Proietti. An integrated study for mapping the moisture distribution in an ancient damaged wall painting. *Anal Bioanal Chem*. 2009; 395: 2245-2253.
[5] L Senni, M Caponero. Moisture content and strain relation in wood by Bragg grating sensor and unilateral NMR. *Wood. Sci. Technol.* 2010; 44: 165-175.
[6] E Del Federico, Silvia A. Centeno. Unilateral NMR applied to the conservation of works of art. *Anal. Bioanal. Chem.* 2010; 396: 213-220.
[7] P Pourmand, Lin Wang. Assessment of moisture protective properties of wood coatings by a portable NMR sensor. *J. Coat. Technol. Res.* 2011; 8 (5): 649-654.
[8] A Masic, MR Chierotti. Solid-state and unilateral NMR study of deterioration of a Dead Sea Scroll fragment. *Anal. Bioanal. Chem*. 2011; 9(3): 234-241.
[9] N Proietti, F Presciutti. Unilateral NMR 13C CPMAS NMR spectroscopy and micro-analytical techniques for studying the materials and state of conservation of an ancient Egyptian wooden sarcophagus. *Anal. Bioanal. Chem*. 2011; 399: 3117-3131.
[10] Blumich, J Perlo. Mobile single-sided NMR. *Progress in Nuclear Magnetic Resonance Spectroscopy*. 2008; 52: 197-269.
[11] H Raich, P Blumler. Design and Construction of a Dipolar Halbach Array with a Homogeneous Field from Identical Bar Magnets: NMR Mandhalas. *Magn. Reson Engineering*. 2004; 23B: 16-25.
[12] Jinghui Liang, Xiaofeng Zhang, Mingzhong Qiao, Geng Li. Multi-field coupling analysis of integrated motor propulsor. *TELKOMNIKA Indonesian Journal of Electrical Engineering*. 2012; 10(7): 1897-1903.
[13] PM Glover, PS Aptaker. A Novel High-Gradient Permanent Magnet for the Profiling of Planar Films and Coatings. *Journal of Magnetic Resonance*. 1999; 139: 90-97.
[14] Prasad, Pottumarthi V. Magnetic resonance imaging: methods and biologic applications. Biswas Hope press. 2006.
[15] Wu Xiaowen, Shu Naiqiu, Li Hongtao, Li Ling. Thermal analysis in gas insulated transmission lines using an improved finite-element model. *TELKOMNIKA Indonesian Journal of Electrical Engineering.* 2013; 11(1): 458-467.
[16] Xinhua Yi, Mingjun Wang, Xiaomin Cheng. Deformation sensing of colonoscope on FBG sensor net. *Telkomnika*. 2012; 10(8): 2253-2260.